Clinical Neurophysiology xxx (xxxx) xxx

Contents lists available at ScienceDirect

Clinical Neurophysiology

journal homepage: www.elsevier.com/locate/clinph

Microscale dynamics of electrophysiological markers of epilepsy

Jimmy C. Yang [a,b], Angelique C. Paulk [b], Pariya Salami [b], Sang Heon Lee [d], Mehran Ganji [d], Daniel J. Soper [b], Daniel Cleary [c], Mirela Simon [b], Douglas Maus [b], Jong Woo Lee [e], Brian V. Nahed [a], Pamela S. Jones [a], Daniel P. Cahill [a], Garth Rees Cosgrove [f], Catherine J. Chu [b], Ziv Williams [a], Eric Halgren [g], Shadi Dayeh [d], Sydney S. Cash [b,*]

[a] Department of Neurosurgery, Massachusetts General Hospital, 55 Fruit St., Boston, MA 02114, USA
[b] Department of Neurology, Massachusetts General Hospital, 55 Fruit St., Boston, MA 02114, USA
[c] Department of Neurosurgery, University of California, San Diego; 9500 Gilman Dr., La Jolla, CA 92093, USA
[d] Department of Electrical and Computer Engineering, University of California, San Diego; 9500 Gilman Dr., La Jolla, CA 92093, USA
[e] Department of Neurology, Brigham and Women's Hospital, 60 Fenwood Rd., Boston, MA 02115, USA
[f] Department of Neurosurgery, Brigham and Women's Hospital, 60 Fenwood Rd., Boston, MA 02115, USA
[g] Department of Radiology, University of California, San Diego; 9500 Gilman Dr.; La Jolla, CA 92093, USA

ARTICLE INFO

Article history:
Accepted 29 June 2021
Available online xxxx

Keywords:
Microelectrode
Interictal Discharges
High Frequency Oscillations

HIGHLIGHTS

- PEDOT:PSS microelectrodes with 50 μm spatial resolution uniquely reveal spatiotemporal patterns of markers of epilepsy.
- High-resolution recording can track interictal discharges and reveal cortical domains involved in microseizures.
- High frequency oscillations detected by microelectrodes demonstrate localized clustering on the cortical surface.

ABSTRACT

Objective: Interictal discharges (IIDs) and high frequency oscillations (HFOs) are established neurophysiologic biomarkers of epilepsy, while microseizures are less well studied. We used custom poly(3,4-ethylenedioxythiophene) polystyrene sulfonate (PEDOT:PSS) microelectrodes to better understand these markers' microscale spatial dynamics.
Methods: Electrodes with spatial resolution down to 50 μm were used to record intraoperatively in 30 subjects. IIDs' degree of spread and spatiotemporal paths were generated by peak-tracking followed by clustering. Repeating HFO patterns were delineated by clustering similar time windows. Multi-unit activity (MUA) was analyzed in relation to IID and HFO timing.
Results: We detected IIDs encompassing the entire array in 93% of subjects, while localized IIDs, observed across < 50% of channels, were seen in 53%. IIDs traveled along specific paths. HFOs appeared in small, repeated spatiotemporal patterns. Finally, we identified microseizure events that spanned 50–100 μm. HFOs covaried with MUA, but not with IIDs.
Conclusions: Overall, these data suggest that irritable cortex micro-domains may form part of an underlying pathologic architecture which could contribute to the seizure network.
Significance: These results, supporting the possibility that epileptogenic cortex comprises a mosaic of irritable domains, suggests that microscale approaches might be an important perspective in devising novel seizure control therapies.

* Corresponding author at: Massachusetts General Hospital, Their 423; 55 Fruit St., Boston, MA 02114, USA.
E-mail address: scash@partners.org (S.S. Cash).

https://doi.org/10.1016/j.clinph.2021.06.024
1388-2457/

1. Introduction

Interictal discharges (IIDs) are neurophysiologic abnormalities that are the hallmark of the epileptic brain, though their cellular underpinnings and relationship to ultimate clinical outcome continue to be debated (Dworetzky and Reinsberger, 2011; Wilke et al., 2009). Similarly, high frequency oscillations (HFOs) have been identified in pathologic regions of cortex and are hotly pursued as possible key biomarkers for ictogenic cortical regions (Burnos et al., 2016; Cimbalnik et al., 2018; Jacobs et al., 2018; Jefferys et al., 2012; Worrell and Gotman, 2011). The intersection of these two markers, known as IID-ripples, have also been identified as potentially more specific markers for seizure onset zones (van Klink et al., 2016; Wang et al., 2013), and IID-ripple resection correlates with improved post-surgical outcome (Wang et al., 2017, 2013). In parallel, some studies have reported on microseizures as another form of epileptiform activity that may indicate the seizure onset zone (Stead et al., 2010).

IIDs, HFOs, and microseizures have all been described on the scale of millimeters to centimeters, but the actual spatial scale of epileptiform activity and the precise structures of the pathological networks underlying such activity remain unknown. However, recent advances in microelectrode technology have revealed previously hidden details of IIDs and seizures, including the micron-level spatial appearance of events. High-spatial-resolution recordings obtained using penetrating or surface electrodes arranged in a grid have suggested that interictal and ictal activity can be generated from small areas 200 μm^2 (micrometers^2) in size (Keller et al., 2010; Schevon et al., 2008; Stead et al., 2010) , though even these studies did not define the lower spatial limit of epileptiform activity.

Progress in microelectrode technologies has increased flexibility in electrode arrangement and spatial resolution, which may be the key to understanding the precise spatiotemporal scale of epileptiform activity. Studies have explored using organic electrode materials such as poly(3,4-ethylenedioxythiophene) polystyrene sulfonate (PEDOT:PSS), which can be lithographically patterned onto flexible parylene C substrates to record neural activity (Khodagholy et al., 2016, 2015). These devices are comprised of micron-level electrode contact sizes that enable high spatial resolution while retaining low impedance (20–30 kilo-Ohms (kΩ)) and close surface conformability (Khodagholy et al., 2015). Such high-spatial-resolution systems can reduce spatial averaging effects and thus examine highly localized phenomena (Harrach et al., 2020; Wellman et al., 2018).

We hypothesized that PEDOT:PSS microelectrodes, which have higher spatial resolution, would reveal not only interictal activity microdomains but also epileptiform activity dynamics that may not have been previously detected by microelectrodes with lower spatial resolution. To test this, we used two different microelectrode designs to examine high-spatial-resolution neural activity in 30 subjects and found evidence that local microdomains can demonstrate epileptiform activity.

2. Methods

2.1. Subjects

Intraoperative recordings were performed in subjects who underwent a neurosurgical procedure at Massachusetts General Hospital (MGH) or Brigham and Women's Hospital (BWH). Patients aged 18 to 70 were approached if they were already scheduled for surgery to remove a lesion (such as a tumor, vascular malformation, or seizure focus). A subset of patients underwent awake cognitive testing with or without electrocorticography (intracranial EEG) during surgery. The possibility of conducting research recordings was only discussed with the patient after the decision to move ahead with surgery had been made. Patients who were medically unstable or who required emergency or urgent surgery were not enrolled in this study. In addition, patients in whom the brain tissue to be removed was expected to be largely dysfunctional (as in the case of large tumors that involved superficial cortex) were not enrolled. These decisions were made in consultation with the treating neurosurgeon and were aimed at excluding patients in whom the surgery would be unusually complicated or from whom the likelihood of obtaining a good-quality neural activity recording would already be compromised. Further, patients with clearly impaired decision-making abilities (as determined by the primary clinical team or physician caring for the patient) were not recruited. In order to limit the study's potential risks to subjects, such as additional operative time, anesthesia, and potential discomfort, the time allowed for dedicated research recording was limited per subject. This study was approved by the Partners Institutional Review Board (now the Mass General Brigham Institutional Review Board), which covers both MGH and BWH. All subjects participated voluntarily, provided informed consent, and were informed that participation in the study would not alter their clinical treatment in any way and that they could withdraw at any time without altering their clinical care.

2.2. Physiological manipulations

In the course of the surgery and as part of routine clinical care, cold saline was applied to reduce epileptiform activity in a subset of subjects (N = 8). We recorded activity via the microelectrodes during cold saline application to detect waveform activity changes through time. In addition, in another subset of subjects (N = 9), we recorded neural activity during intravenous injection of medication that was used to activate epileptiform abnormalities as part of the patients' intraoperative clinical management. We recorded neural activity before (baseline) and for up to 5 minutes after the intervention.

Fig. 1. Microelectrode Characteristics. A) Two poly(3,4-ethylenedioxythiophene) polystyrene sulfonate (PEDOT:PSS) electrode designs used, with intraoperative images. Top row shows the bi-linear array comprised of two rows of 64 30 μm-contacts, with 50 μm spacing. The entire length of the electrode is 3150 μm (center-to-center). Bottom row shows the circular grid, comprised of seven rings at varying distances from the center. Intraoperative photograph shows both electrode types (cyan boxes) on the cortical surface. B) Three-dimensional reconstruction of a subject's brain, with overlaid putative positions of clinical strip electrodes (blue contacts) and PEDOT:PSS bi-linear array (orange contacts). The bi-linear array (shown in orange) is the two small lines in the expanded middle and left panels. The clinical contacts are marked by blue circles above and below the PEDOT:PSS array. The two larger orange circles and the two orange squares are localizing markers to indicate electrode placement and allow for photographic alignment of the recordings (see (A)). C) Comparison of clinical recording vs. PEDOT:PSS experimental recording, spectral power through time (Top: clinical recording, Bottom: PEDOT:PSS recording). D) Comparison of clinical recording vs. PEDOT:PSS experimental recording, ten seconds of voltage dynamics, with IIDs observable in both recordings (Blue: clinical recording, Red: PEDOT recording). E) Different referencing of the neural signal preserve underlying recorded signals. Upper traces over 1 second (red and magenta) show raw and bipolar re-referenced clinical recordings, while lower traces (blue, green, and black) show raw versions of the common average vs. bipolar re-referenced PEDOT:PSS recordings. Abbreviations: PEDOT – poly(3,4-ethylenedioxythiophene) polystyrene sulfonate; m – meters; Hz – hertz; V – volts; s – seconds.

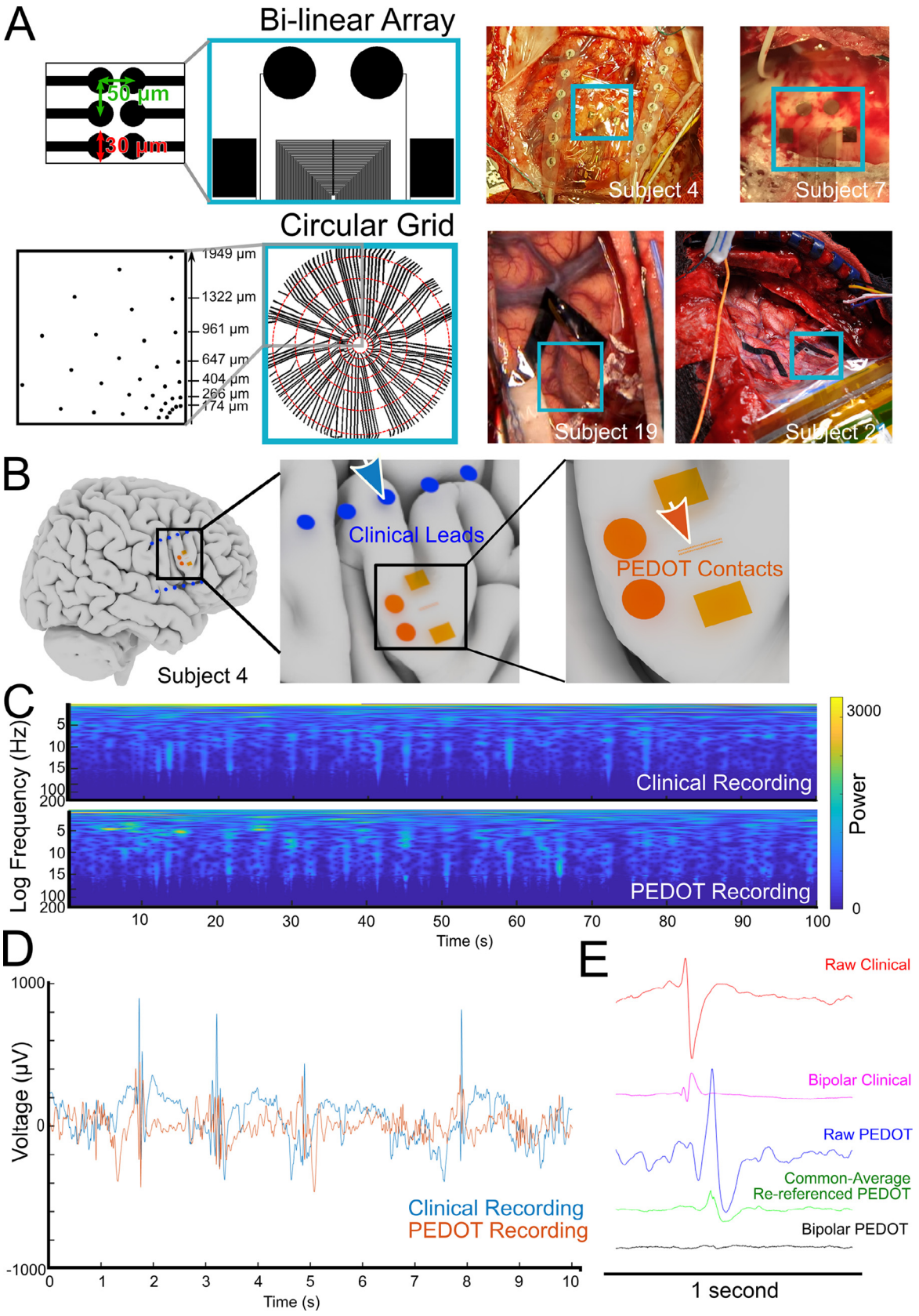
A
Bi-linear Array
50 µm
130 µm
Subject 4
Subject 7
Circular Grid
1949 µm
1322 µm
961 µm
647 µm
404 µm
266 µm
174 µm
Subject 19
Subject 21
B
Clinical Leads
PEDOT Contacts
Subject 4
C
Log Frequency (Hz)
Clinical Recording
PEDOT Recording
Power
3000
0
Time (s)
D
Voltage (µV)
Clinical Recording
PEDOT Recording
Time (s)
E
Raw Clinical
Bipolar Clinical
Raw PEDOT
Common-Average Re-referenced PEDOT
Bipolar PEDOT
1 second

2.3. Device manufacture

The PEDOT:PSS device was fabricated similarly to previous protocols described elsewhere (Ganji et al., 2018; Sessolo et al., 2013). This study used two different electrode designs. One was organized as a bi-linear array comprising 128 channels arranged in two columns (each column had 64 channels), with an electrode diameter of 30 μm and interelectrode center-to-center distance of 50 μm. A second design employed a circular grid, with electrodes arranged in concentric rings at varying distances from the center (Fig. 1**A**). Including both electrode types allowed us to test whether the bi-linear array (the first design used) or the circular grid could be better optimized for sampling IID and HFO propagation and spread. The bi-linear array was able to investigate maximum cortex length, in case specific microdomain boundaries could be detected. The circular grid's gradually increasing distances between rings maximized spatial coverage. Both electrode types detected our targeted events, and the circular grid enabled wide sampling of the signal at different spatial scales.

2.4. Data acquisition and processing

Intraoperative research recordings from PEDOT:PSS electrodes were obtained using an Intan recording system with a sampling

Table 1
Subject and recording characteristics. Abbreviations: MAC – monitored anesthesia care; General – General Anesthesia; Linear – bi-linear PEDOT:PSS electrode design; Circular – circular PEDOT:PSS electrode design; Cold Saline – cold saline applied during the procedure; Inducing medication – medication to induce epileptiform activity.

Subject #	Age	Handedness	Type of Case	History of Seizure	Anesthesia Type	Electrode type	Inducing Medication	Cold Saline	Recording Length (Seconds)
1	33	Right	Left temporal lobectomy for seizure	Yes	General	Linear	Methohexital		1250
2	37	Right	Right temporal lobectomy for seizure	Yes	General	Linear	Methohexital		628
3	22	Right	Right temporal lobectomy for seizure	Yes	General	Linear	Methohexital		717
4	24	Right	Right temporal lobectomy for seizure	Yes	General	Linear			1213
5	43	Left	Right temporal lobectomy for seizure	Yes	General	Linear	Methohexital		941
6	29	Right	Right temporal lobectomy for seizure	Yes	General	Linear	Methohexital		1377
7	44	Right	Right redo temporal lobectomy for seizure	Yes	General	Linear	Methohexital		1501.5
8	39	Right	Right temporal lobectomy for seizure	Yes	General	Circular	Methohexital	Yes	2205
9	37	Right	Left parietal tumor resection	Yes	MAC	Linear			445
10	40	Right	Right temporal lobectomy for seizure	Yes	General	Linear		Yes	544.5
11	42	Right	Right temporal lobectomy for seizure	Yes	General	Linear	Alfentanil		1003
12	25	Left	Right redo parietal resection for seizure	Yes	General	Linear			348
13	62	Right	Left temporal tumor resection	Yes	MAC	Linear			715
14	39	Right	Right parietal tumor resection	Yes	General	Linear			301
15	36	Right	Left redo temporoparietal resection for seizure	Yes	MAC	Linear		Yes	346
16	22	Right	Right temporal lobectomy for seizure	Yes	General	Linear			844.5
17	52	Right	Left temporal craniotomy for AVM	Yes	MAC	Linear			887.5
18	29	Left	Right redo parietal resection for seizure	Yes	General	Circular			1191
19	55	Left	Right temporal tumor resection	No	MAC	Circular		Yes	961
20	48	Right	Right temporal lobectomy for seizure	Yes	General	Circular			546.5
21	33	Right	Right frontal lobectomy for seizure	Yes	General	Circular		Yes	1901.5
22	53	Right	Left craniotomy for tumor	Yes	MAC	Linear		Yes	600 785
23	32	Right	Left craniotomy for tumor	No	MAC	Circular		Yes	785
24	52	Right	Right temporal lobectomy for seizure	Yes	General	Circular		Yes	1370.5
25	57	Right	Right temporal lobectomy for seizure	Yes	General	Circular	Alfentanil		975.6
26	22	Left	Left modified hemispherectomy	Yes	General	Circular			377.6 941.8
27	24	Right	Right temporal lobectomy for seizure	Yes	General	Circular			798
28	64	Right	Left craniotomy for tumor	Yes	MAC	Linear			945.2
29	55	Right	Left temporal lobectomy for seizure	Yes	MAC	Linear			106 1760 521.2
30	36	Right	Left frontal craniotomy for seizure	Yes	MAC	Circular			1358.3 687.7

rate of 30 kilo-Hertz (kHz) (bandpass filtered from 1 Hz to 7500 Hz, with the low pass filter to reduce aliasing), as described previously (Hermiz et al., 2016). During acquisition, ground and reference needle electrodes (Medtronic, Minneapolis, MN, USA) were placed in nearby tissue, normally in muscle or scalp. After electrode placement on brain tissue, impedance testing was performed for 30 seconds using the Intan RHD2000 software. Once the software was closed, we recorded neural activity using OpenEphys, an open-source electrophysiology software suite. OpenEphys allowed for PEDOT:PSS microelectrode recording and visualization across all channels along with analog triggers to enable signal synchronization (Siegle et al., 2017).

As these recordings were all intraoperative, recording duration was limited to minutes so as to avoid extending the surgery and to reduce overall risk to the participants. Subjects were under either general anesthesia or monitored anesthesia care (MAC) during the recordings, depending on clinical indication (Table 1). The choice to use the bi-linear versus circular electrode design for each subject was based on electrode availability (as electrodes were manufactured in batches), whether a particular case could provide insights into IID and HFO spread or localization, and if a cognitive task would be performed (for a separate study; (Paulk et al., 2021)). As electrodes' spatial resolution were comparable between designs (Fig. 1**A**), we found we could measure dynamics across electrodes.

When used, intracranial intraoperative clinical electrocorticography or depth electrode recordings were performed simultaneously using PMT or Ad-tech electrodes (Ad-tech Medical, Racine, WI, USA, or PMT, Chanhassen, MN, USA). In general, at BWH, Ad-tech clinical strip platinum electrodes utilized 10 mm spacing and 2.3 mm contact diameter, while Ad-tech depth platinum electrodes employed 5–8 mm spacing, 2.41 mm contact size, and 1.12 mm diameter. At MGH, PMT Cortac clinical strip platinum electrodes used 10 mm spacing, 3 mm contact diameter, and PMT Depthalon depth platinum electrodes had 3.5 mm spacing, 2 mm contacts, and 0.8 mm diameter. The neurosurgeon placed clinical electrodes in the regions of clinical interest. Clinical electrode recordings – and no other recording types – used the Natus Quantum system (Natus Neurology Inc., Middleton, WI, USA); the clinical team dictated sampling rates, which were typically at either 4096 or 512 Hz.

2.5. Data analysis and data exclusion criteria

To detect events, we performed data analysis on the microelectrode (PEDOT:PSS) recordings using custom MATLAB scripts. Raw voltage signals were taken directly from the OpenEphys recordings. We scrutinized recordings and channels for potential noise, produced by the intraoperative environment, that would alter analyses. Channels with excessive line noise, artifacts, or high impedances (>100 kΩ) were removed from analysis (Paulk et al., 2021). Recordings from three subjects were removed due to substantial movement artifacts. While examining the high-frequency domain for analyzing HFOs, three additional recordings were removed due to high-frequency electrical noise, likely caused by the intraoperative environment, that could not be suppressed. Following these exclusions, HFO-related analyses included 24 subjects.

For further analyses, we used either the referential data or filtered referential data. We found that re-referencing the microelectrode data using common average re-referencing or bipolar re-referencing did not completely eliminate the observed large events, such as interictal discharges (Fig. 1**E**). However, as expected, bipolar re-referencing tended to remove relevant signals from events that spanned the electrode, likely due to the high spatial resolution of the microelectrodes themselves.

2.6. Detecting and mapping interictal discharges (IIDs)

Before conducting IID detection and analysis, local field potential (LFP) data were decimated to 1000 Hz and demeaned relative to the entire recording. To remove 60 Hz noise (and associated harmonics), second-order Butterworth bandpass filters for 60 Hz (58–62 Hz band), 120 Hz (118–122 Hz band), and 180 Hz (178–182 Hz band) were calculated in MATLAB and subsequently subtracted from the raw signal.

IIDs were automatically detected using a published algorithm that first filters the data into a 10–60 Hz band, then applies an envelope, and finally finds an appropriate threshold value modeled on a statistical distribution in the sampled envelope (Janca et al., 2015). We then reviewed each detection visually. Each IID was classified as either a general event, if it was seen across > 50% of channels, or a local event, seen across $\leq$ 50% of channels. For local IIDs, we also calculated the minimal detection distance based on the spacing of the microelectrode contacts, which have known Euclidian distances from each other. Signal presence on specific electrodes, but not on neighboring electrode contacts, was used as a proxy to define the minimal cortical range or "distance" required for IID generation.

In recordings with at least ten IIDs, we peak tracked the propagating IID across the electrode grids by finding the maximum or minimum voltage value and associated time for each interictal discharge event on each channel per IID event. This method provided that event's three-dimensional path, through time, across the x and y positions of the microelectrode contacts over a specified two-second time window, with the third dimension representing time as the IID traversed the electrode. The two-second time window ensured we did not clip any possible path information. The discrete Fréchet distance between event pairs was subsequently calculated to determine path similarity between each IID event pair (Eiter and Mannila, 1994), using open-source software (https://www.mathworks.com/matlabcentral/fileexchange/31922-discrete-frechet-distance). In brief, Fréchet distance measures similarity between any two paths obtained by calculating, and minimizing, the difference between them, resulting in an approximation using sampled points along each curve. Path similarity between every IID event pair was measured across the same electrode array per recording (and not compared across recordings). As Fréchet distance is a point-by-point comparison between paths, it is not as susceptible to differences in electrode spacing or distributions (methodology illustrated in Fig. 2**F, 2H**).

Next, these pairwise values were clustered by evaluating solutions provided by the evalclusters MATLAB agglomerative clustering algorithm, which used a silhouette clustering evaluation criterion based on a cosine distance metric in order to maximize vector differences between clusters. This function's output identified the optimal number of clusters by evaluating the CriterionValues field. After clustering the IID paths (where each path represents a group of similar IIDs from a single recording, in a single subject), the cluster's mean coordinate was calculated for each point in time, and a smoothed mean over 10 ms was applied to visualize that clustered group's average trajectory.

2.7. Detecting and mapping high frequency oscillations (HFOs)

To detect HFOs, raw data were decimated to 2000 Hz and bandpassed in a frequency range of 80–200 Hz for the ripple band and 250–500 Hz for the fast ripple band, as previously reported (Lévesque et al., 2012; Salami et al., 2012). The decision to decimate the data to 2000 Hz was based on prior studies that suggested using a sampling rate of 2000 Hz or greater to detect HFOs (Gliske et al., 2016). Furthermore, in a subset of eight sub-

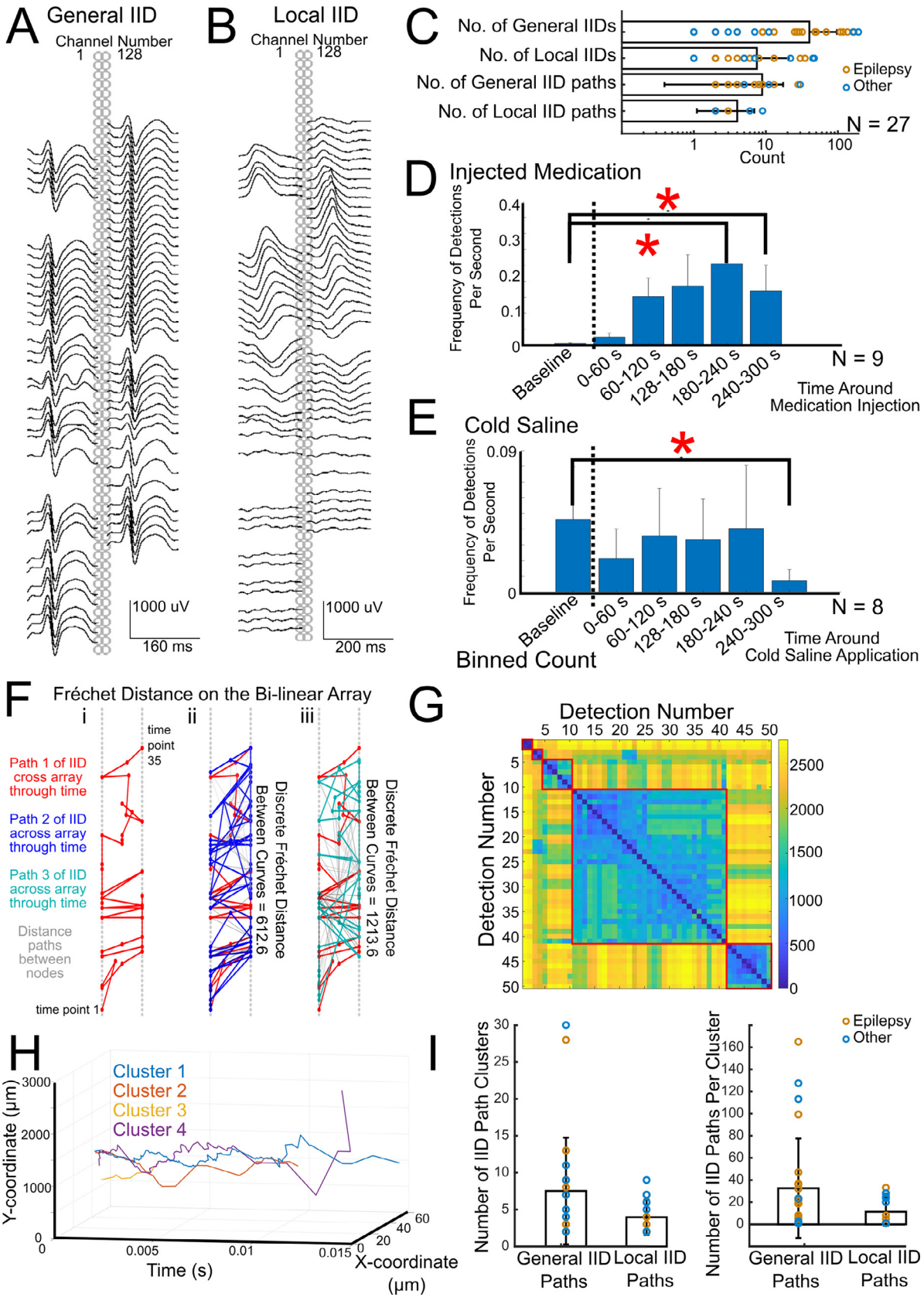
A
General IID
Channel Number
1
128
1000 uV
160 ms
B
Local IID
Channel Number
1
128
1000 uV
200 ms
C
No. of General IIDs
No. of Local IIDs
No. of General IID paths
No. of Local IID paths
Epilepsy
Other
N = 27
1
10
100
Count
D
Injected Medication
Frequency of Detections Per Second
0.4
0.3
0.2
0.1
0
Baseline
0-60 s
60-120 s
128-180 s
180-240 s
240-300 s
N = 9
Time Around Medication Injection
E
Cold Saline
Frequency of Detections Per Second
0.09
0
Baseline
0-60 s
60-120 s
128-180 s
180-240 s
240-300 s
N = 8
Time Around Cold Saline Application
Binned Count
F
Fréchet Distance on the Bi-linear Array
i
ii
iii
time point 35
time point 1
Path 1 of IID cross array through time
Path 2 of IID across array through time
Path 3 of IID across array through time
Distance paths between nodes
Discrete Fréchet Distance Between Curves = 612.6
Discrete Fréchet Distance Between Curves = 1213.6
G
Detection Number
5 10 15 20 25 30 35 40 45 50
Detection Number
2500
2000
1500
1000
500
0
H
Cluster 1
Cluster 2
Cluster 3
Cluster 4
Y-coordinate (μm)
3000
2000
1000
0
0
0.005
0.01
0.015
Time (s)
0
20
40
60
X-coordinate (μm)
I
Number of IID Path Clusters
30
25
20
15
10
5
0
General IID Paths
Local IID Paths
Number of IID Paths Per Cluster
160
140
120
100
80
60
40
20
0
Epilepsy
Other
General IID Paths
Local IID Paths

jects, we compared HFO frequency per channel, using data decimated to either 2000 Hz or 5000 Hz, to determine whether decimation to 2000 Hz affected the overall frequency of HFO detections. We found no statistically significant difference in the overall frequency of HFO detections between the two sampling rates (Wilcoxon Rank-Sum test, $p > 0.05$).

The HFO detection algorithm (Lévesque et al., 2012; Salami et al., 2012) uses a reference time window to detect peaks in the filtered data. For our analysis, the reference time window was selected from a recording segment that appeared to be free from artifacts such as movement. A detection must have at least four oscillations to be considered an HFO. To avoid artifacts and false detections, only fast ripples that did not overlap with lower-frequency ripples were considered detections. In other words, we rejected fast ripples that coincided with lower-frequency ripples to ensure we focused on the putatively more pathologic fast ripples. We chose to focus on fast ripples based on prior research that suggested fast ripples seen on microelectrodes can be associated with epileptogenicity or ictal onsets (Bragin et al., 2002a; Chari et al., 2020; Weiss et al., 2016; Worrell et al., 2008; Zijlmans et al., 2012b). Each channel was also visually reviewed to validate and verify the oscillatory waveforms and to check the raw recordings to confirm the oscillations were not due to sharp large voltage events. Overall, detections were at least 2.9 standard deviations above the mean when addressing the amplitude criterion for the detector.

To determine the spatial similarity of detected HFO events over the microelectrode array throughout the recording, we adapted an approach that has been previously used to identify and characterize neural avalanches (Beggs and Plenz, 2004; Ribeiro et al., 2016). This method uncovered spatial and temporal patterns that could otherwise be missed. In brief, we first calculated the average time between HFO detections. Preliminary analysis indicated that creating a small time window would oversimplify patterns by grouping few HFO detections per time window. As a result, we chose a time window 5 standard deviations longer than the average time between HFO detections. Though any time window length selected would arbitrarily group the HFO detections, we ultimately relied on statistical testing (see below) to determine if any grouped detections were unique in a statistically significant manner. For each time window (subdivided from total recording time), a microelectrode contact was designated "1" if an HFO was detected and "0" if no HFO was detected. We then calculated a similarity index between time window arrays as defined by $Sim(A,B) = |A \cap B| / |A \cup B|$; this index divides the total number of co-occurring detections between the time windows by the total number of unique electrode detections (methodology illustrated in Fig. 3E). These similarity indices between time windows were then clustered using a paired clustering algorithm, based on Euclidean distance, leading to "families" of time windows with optimal similarity. Clustering was performed using the MATLAB cluster function at each dendrogram level that had allowed each family to be grouped. Put another way, we determined clustering at each level, ranging from 1 to the total number of time windows. Next, we calculated the contrast function at each dendrogram level as $C = (D_{in} - D_{out})/(D_{in} + D_{out})$ (Beggs and Plenz, 2004). This function compares the similarity values found within the clustered families (D_{in}), versus those outside the families (D_{out}), to maximize within-family similarity values. We could then plot the contrast function and evaluate local maxima as clustering solutions (Fig. 3**E**).

Our next step was to compare the significance of each family to 1,000 shuffled datasets created by randomly permuting the detections per channel in all time frames, which allowed the overall number of active electrodes in each time window to remain constant. Using the same clustering method as for the actual data, as detailed above, we then calculated the probability of obtaining a family of a given size and average similarity. Finally, we implemented the Benjamini-Hochberg multiple comparisons correction (Ribeiro et al., 2016).

2.8. Identifying periodic discharges and microseizures

Visually reviewing the entire recording, with guidance from the IID methodology described above, identified periodic discharges and microseizures. In accordance with the clinical literature, we defined periodic discharges as paroxysmal complexes that occurred at a relatively stable frequency, lasted $\geq$ 0.5 seconds but < 10 seconds, and had a frequency that was typically $\leq$ 4 Hz (Ebersole, 2014; Hirsch et al., 2021). Further, we defined microseizures as either an epileptiform discharge pattern lasting $\geq$ 10 seconds with a frequency of > 2.5 Hz or an evolving pattern lasting $\geq$ 10 seconds (Ebersole, 2014; Hirsch et al., 2021) (as illustrated in Fig. 4**C, 4E**).

2.9. Evaluating Multi-Unit activity (MUA)

Because the intraoperative environment had the potential to introduce several artifact sources, we examined MUA as the synthesis of sorted fast unitary events. This had the advantage of also decreasing the likelihood that high frequency oscillation filtering could be detected as MUA. Fast unitary waveform events were first sorted using single unit sorting approaches. Then, the events were pooled per recording into MUA. The fast single unit-like waveforms (0.2–0.5 microseconds in duration) were detected and sorted into waveform clusters using Kilosort (Pachitariu et al., 2016). Kilosort detects high-frequency waveforms and clusters them based on both waveform shape and spatial mapping on the electrode grid. We were able to recognize repeated (but not rhythmic) waveform

Fig. 2. Interictal Discharges (IIDs). A) Example of a general interictal discharge seen over the entire poly (3,4-ethylenedioxythiophene) polystyrene sulfonate (PEDOT:PSS) bi-linear array, with low pass filtering as described in Methods. Electrode channel numbers 1 and 128 are indicated. This represents one example of many (see Table 2). B) Example of a local interictal discharge seen only over a portion of the PEDOT:PSS bi-linear array, organized in the same way as (A). This represents one example of many (see Table 2). C) Counts of General IIDs, Local IIDs, General IID paths, and Local IID paths per participant (scatter plots) and mean counts across participants (bar graph and standard deviation error bars). D) Histogram showing interictal discharge responses to activating medications (methohexital or alfentanil), N = 9 treated subjects, with standard deviation error bars. * indicates $p < 0.05$ (Wilcoxon Rank-Sum). Baseline refers to the IID frequency per second prior to medication injection (to the left of the dashed vertical line). Five time bins to the right of the vertical dashed line illustrate detection frequency in the time bin as described on the x-axis. E) Interictal discharge responses to cold saline irrigation, N = 8 treated subjects, with standard deviation error bars. * indicates $p < 0.05$ (Wilcoxon Rank-Sum). Histogram is organized as described in (D). F) Fréchet distances between two paths. i) is an example path, and ii) shows two overlaid paths, with gray lines indicating measurements between node points in two paths, resulting in the discrete Fréchet distances indicated to the right. iii) depicts two more overlaid paths with a different discrete Fréchet distance value. Gray dots represent the actual bilinear PEDOT:PSS 128-channel array, and the color-coded paths are the actual peak tracked data for three different general IID events in a single subject. G) Example of clustering by Fréchet distance. Color-coding indicates the calculated Fréchet distance. Each detection represents one IID, which is paired to another IID within the subject to generate the calculated Fréchet distance value. H) Four clustered families' paths over the electrode, and mean vector for each family represented in three-dimensional space. I) Left: Number of clusters identified per patient (in the scatter plots) and averaged across patients (bar and standard deviation error bar plot). Right: Average number of IID paths per cluster for the General and Local IID paths. Note: For (A) and (B), voltage tracings not shown represent electrodes that were removed due to exclusion criteria (see 2.5 Data Analysis and Data Exclusion Criteria). Abbreviations: IID – interictal discharge; N – number of subjects; V – volts; m – meters; s – seconds; No. – number.

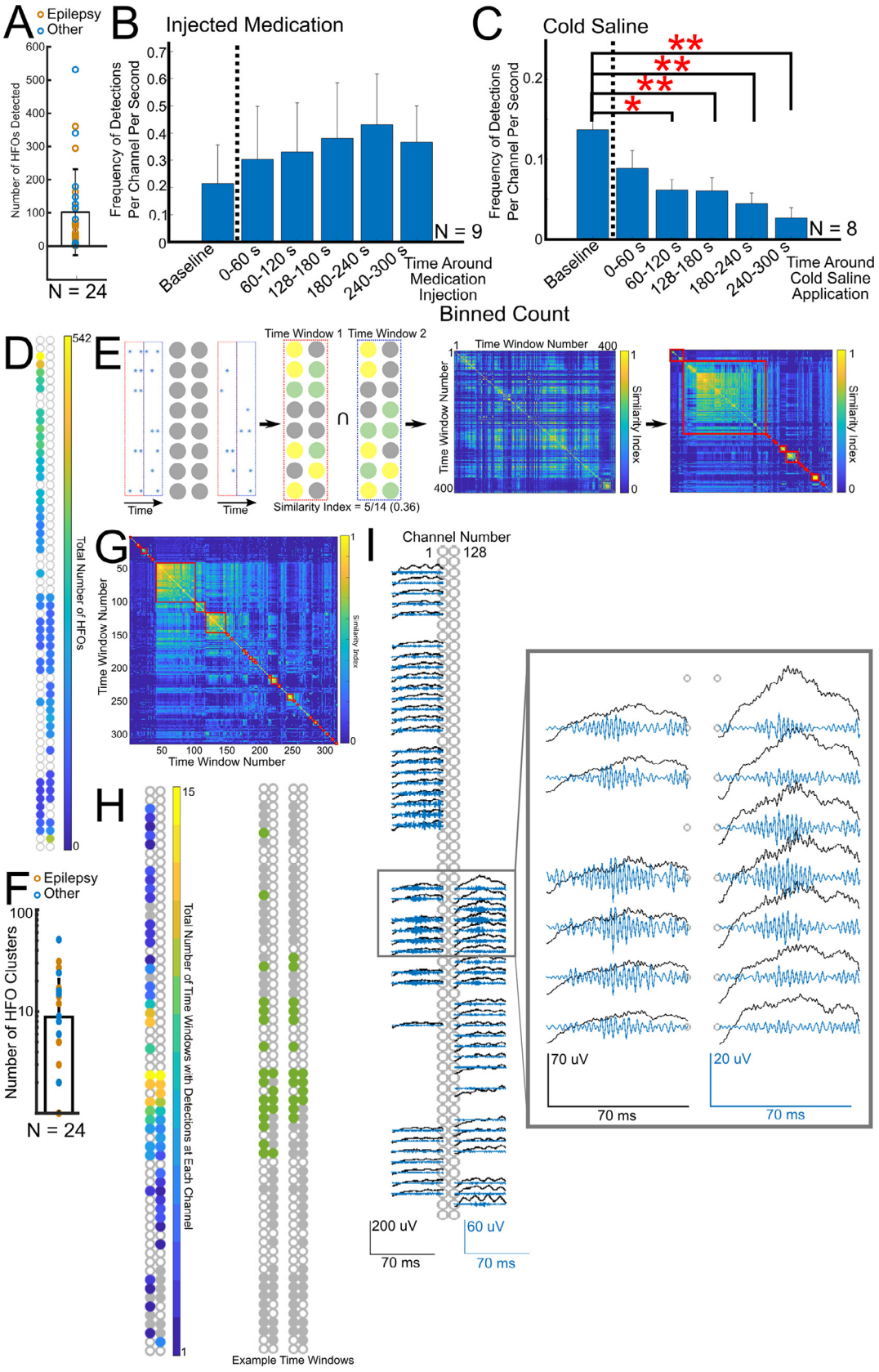
A
Epilepsy
Other
Number of HFOs Detected
N = 24
B
Injected Medication
Frequency of Detections Per Channel Per Second
N = 9
Baseline
0-60 s
60-120 s
128-180 s
180-240 s
240-300 s
Time Around Medication Injection
C
Cold Saline
Frequency of Detections Per Channel Per Second
N = 8
Time Around Cold Saline Application
Binned Count
D
Total Number of HFOs
E
Time Window 1
Time Window 2
Time
Similarity Index = 5/14 (0.36)
Time Window Number
Similarity Index
F
Epilepsy
Other
Number of HFO Clusters
N = 24
G
Time Window Number
H
Total Number of Time Windows with Detections at Each Channel
Example Time Windows
I
Channel Number
70 uV
70 ms
20 uV
200 uV
60 uV

events that could be clustered similarly to typical single-unit spikes. Given that these are recordings from the surface rather than penetrating electrodes, we have been conservative in referring to these events as MUA rather than as single unit discharges which may imply that we are recording action potentials from soma of individual neurons – a possibility which has not yet been proved with these electrodes.

To reduce artifact inclusion, we only applied Kilosort to data with no movement or stimulation artifacts, or we removed noisy channels to detect clear putative clusters of waveform events. Further steps included rejecting waveform clusters that appeared to be artifacts (as with stimulation) or inter-event intervals (IEIs) corresponding to 60 Hz noise, IEIs that were too short (<2ms), and IEIs with highly rhythmic peaks in their distribution. We also identified the waveforms in the raw and original high-pass filtered data to confirm their timing and channel location. Next, we pooled waveform times and confirmed them as fast events similar to MUAs. The reason we did not solely threshold the activity and detect events from the recordings was to be conservative in order to ensure we were measuring what could be isolated MUA activity while eliminating possible artifacts. In addition, this combined approach allowed us to reduce the chance we were detecting HFOs, as the Kilosort algorithm followed by subsequent autocorrelation, cross-correlation rejection, and visual waveform examination specifically filtered out errant, regular, rhythmic oscillatory events in the MUA detections.

2.10. Measuring HFO and IID responses to cold saline and injected medication

To determine if HFO or IID frequency changed with either the application of cold saline or the intravenous injection of medication known to promote IIDs (alfentanil or methohexital), we conducted recordings before and for up to 5 minutes after such manipulations. As a statistical test, we averaged the frequency of HFO, general IID, or local IID events occurring in the minute before the manipulation (baseline) and in 1-minute bins, for a total of 5 minutes, afterward. We then compared the baseline frequency to that of each post-manipulation binned event. This approach allowed us to examine both the effect and time course of changes in the HFO or IID event times. We chose 5 minutes to avoid adding more time to the surgical procedure (see Subjects section above) and because 5 minutes could be consistently recorded across subjects (Table 1).

2.11. Examining covariance between waveform types

To understand if a temporal relationship existed among IIDs, HFOs, and MUA in these microelectrode recordings, we performed covariance calculations for each marker type's times within each data set. Specifically, we completed separate cross-covariance calculations between IID and HFO times, between IIDs and MUA, and between HFOs and MUA. This approach allowed us to first calculate average covariance between event types per patient and then determine average covariance as well as lead and lag times between events across the data set in the microelectrode recordings. For instance, cross-covariance was evaluated by binning the IID rising phase and HFO onset times into milliseconds and then computing cross-covariance between these onsets for a 200 ms period around the IID rising times in the same recordings.

After calculating the mean values of HFO covariance 200 ms both before or after the IID, we used the non-parametric Wilcoxon Rank Sum test to determine whether the central peak was significantly different from a 1-second baseline period that was 5 seconds before the peak across subjects. For comparisons with MUAs, we evaluated covariance 5 seconds either before or after the interictal discharge or HFO, and then we conducted the non-parametric Wilcoxon Rank Sum test to define whether the central peak was significantly different from a 1-second baseline period that was 5 seconds before the peak across subjects. This comparison was done on a per-time-point level (every 0.05 sec) and corrected for multiple comparisons using a false discovery rate control.

3. Results

3.1. Subjects

Thirty subjects participated in PEDOT:PSS microelectrode intracranial intraoperative recordings during their clinical surgical care. The participants, 14 men and 16 women, had a mean age of 39.5 (standard deviation of 12.5) (Table 1). The majority of subjects were right-handed (25), and 22 (73%) underwent a neurosurgical procedure for epilepsy. The remaining patients underwent a neurosurgical procedure for either tumor resection (N =76) or vascular malformation resection (N = 1). Twenty-eight (93%) subjects had prior seizure histories. General anesthesia was used in 20 (67%) subjects, and the rest received monitored anesthesia care (MAC). Of the subjects undergoing a neurosurgical procedure for epilepsy, nine (30%) were treated with medication to activate epileptiform abnormalities as part of their intraoperative clinical management.

Fig. 3. High Frequency Oscillations (HFOs). A) HFO counts per patient (scatter plot) and averaged across patients (bar and standard deviation error bar plots), N = 24. B) Average HFO detection frequency per channel response to activating medications (alfentanil, methohexital), with standard deviation error bars. Baseline refers to IID frequency per second prior to medication injection (to the left of the dashed vertical line). Five time bins to the right of the vertical dashed line illustrate detection frequency in the time bin as described on the x-axis. C) Average HFO detection frequency per channel response to cold saline irrigation, with standard deviation error bars. * indicates $p < 0.05$, ** indicates $p < 0.01$, Wilcoxon Rank-Sum test, N = 8 subjects treated. Figure is organized as described in (B). D) Example of a summative approach to determine if HFOs tend to be detected over specific microelectrode regions, in one recording (one subject). Total HFO detections for each electrode were calculated for the entire recording and are plotted with color-coding. This diagram suggests the top left of the electrode had the most HFOs, but this tends to overlook possible spatiotemporal changes during recording. E) Methodology for spatiotemporal analysis of coordinated HFO detections. Separating HFO detections into specific time windows (see 2.7 Detecting and Mapping High-Frequency Oscillations (HFOs)) identifies "active" electrodes. Red and blue boxes indicate two time-windows in first sub-panel. Boxes to the left correspond to electrodes in the left vertical row, and boxes to the right correspond to electrodes in the right vertical row. Similarity indices between time windows can then be calculated (second sub-panel; yellow electrodes have coincident HFO detections, while green electrodes do not). Similarity indices are illustrated within a matrix (third sub-panel) and subsequently clustered (red boxes) after calculation of the contrast function (see 2.7 Detecting and Mapping High-Frequency Oscillations (HFOs)). ∩: intersection. F) HFO clusters per patient (scatter plot) and averaged across patients (bar and standard deviation error bar plots), N = 24; See Table 2. G) One example of similarity-based clustering by frames (as described in (E) and Methods). H) Example of one clustered frame group from (G). At left is the overall summative detections seen within that family, highlighting that the central part of the microelectrode has more HFOs. Gray circles represent electrodes that did not have HFO detections. The right shows two examples of time windows that were members of this family cluster, with electrodes that had HFO detections in green. Gray circles indicate electrodes that did not have HFO detections. I) Demonstration of one group member seen in (H), with black lines showing raw data decimated to 2000 Hz (see Methods) and blue lines marking the fast ripple filtered band (bandpass filter from 250-500 Hz). Inset shows an array portion in magnified view. Note: For (D), (H), and (I), empty circles represent electrodes that were removed due to exclusion criteria (see 2.5 Data Analysis and Data Exclusion Criteria). Abbreviations: HFO – high frequency oscillation; N – number of subjects; V – volts; s – seconds.

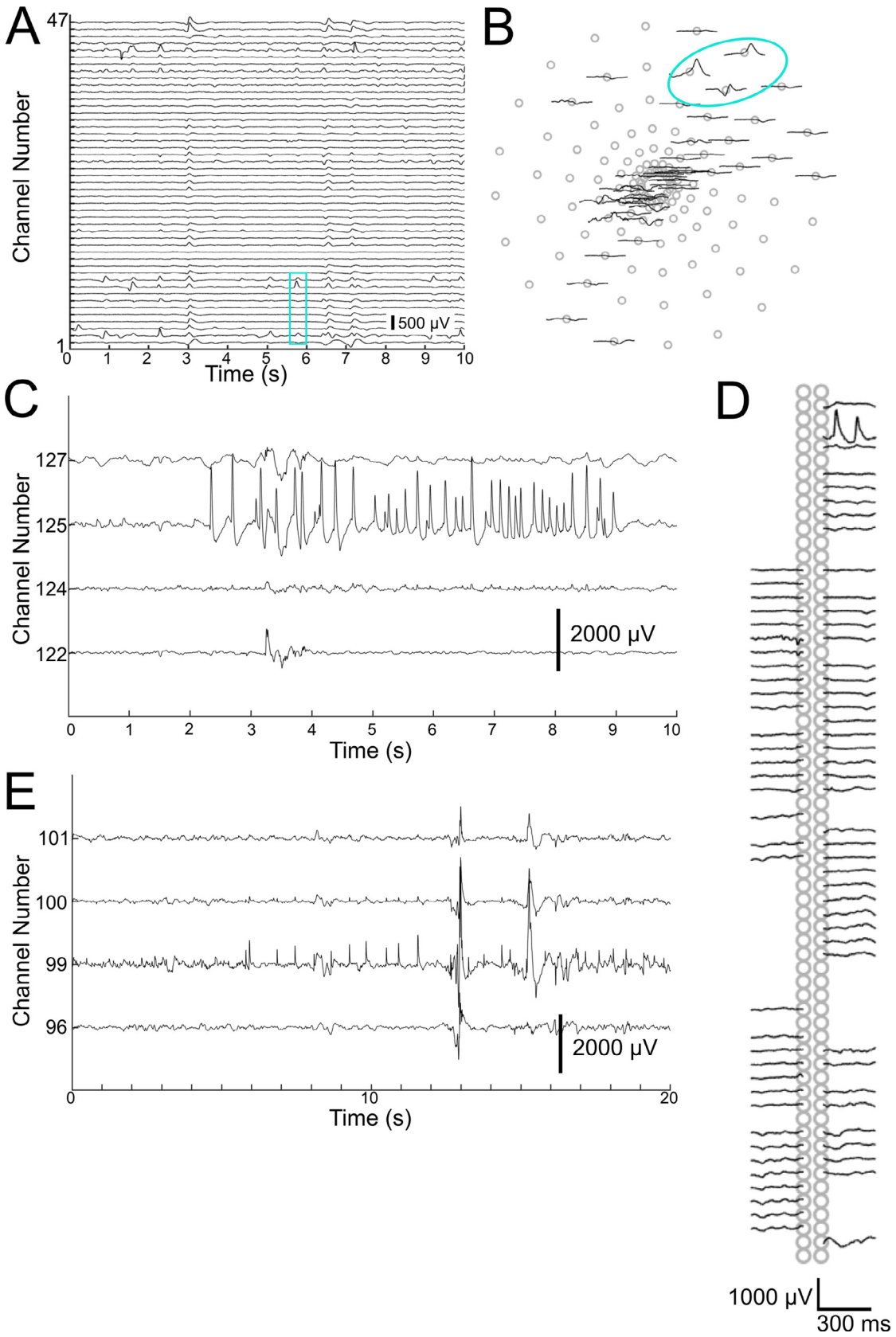

Fig. 4. Periodic Discharges and Microseizure Events in poly(3,4-ethylenedioxythiophene) polystyrene sulfonate (PEDOT:PSS) Microelectrodes. A) Demonstration of one periodic discharge series, seen primarily in channels 6, 13, and 14. Low-pass filtered data are shown, with distance between channels corresponding to 250 μV. B) Spatial location of one periodic discharge series as indicated in the cyan box in A. C) One example of a microseizure event, localized to channel 125. Field can be seen extending to neighboring channels 124 and 127. D) One discharge from C, demonstrated spatially on the bi-linear array. E) Second example of a microseizure event, localized to channel 99. Field can be seen extending to neighboring channel 100. Note: For (B), (C), (D), and (E), voltage tracings not shown represent electrodes that were removed due to exclusion criteria (see 2.5 Data Analysis and Data Exclusion Criteria) Abbreviations: s – seconds; V – volts.

In addition, eight patients had cold saline applied during the procedure to reduce epileptiform activity (Table 1).

Thin film PEDOT:PSS electrodes were used to record neural activity during surgery, sometimes alongside clinical monitoring (Fig. 1). A bi-linear PEDOT:PSS electrode array was used to record neural activity intraoperatively in 20 (67%) subjects, and a circular array was used to record activity in the others (Fig. 1**A**). In each participant, the microelectrode was typically situated on an exposed gyrus within the surgical field, in a location the neurosurgeon considered safe (Fig. 1**B**). Visually comparing concurrent clinical electrocorticography recordings confirmed similar waveforms in the PEDOT:PSS and clinical recordings, with unique features such as IIDs appearing simultaneously in both recordings. Though these are not the main focus of this study, our PEDOT:PSS microelectrode did denote similar neurophysiologic features in the spectral domain (Fig. 1**C**) and voltage dynamics (Fig. 1**D-E**), as has been shown in previous studies (Khodagholy et al., 2015; Paulk et al., 2021) .

3.2. Interictal discharges (IIDs)

IIDs were not only observable across subjects but could also be divided into two types, termed "general" or "local," based on spatial extent. In the PEDOT:PSS recordings, general IIDs were defined as events that, upon visual review of automated detections, occurred over more than 50% of the electrode array (Fig. 2**A**), whereas local IIDs appeared on fewer than 50% of the channels (Fig. 2**B**). General IIDs were seen in 93% of subjects; local IIDs were less frequent but still present in 53% of subjects (Table 2, Fig. 2**C**). Comparing subjects who underwent general anesthesia versus monitored anesthesia care revealed no statistically significant difference in the number of general or local IIDs ($p > 0.05$, Wilcoxon Rank-Sum test). Using the microelectrode contacts as points in Euclidean space, we calculated local IIDs' spatial range across the microelectrode arrays' x and y coordinates. The minimum distance over which a local IID was detected was 50 μm.

Interventions such as cold saline and medications are known to affect the frequency of IIDs and epileptiform activity. As expected, we found that activating medications significantly increased the frequency of general interictal discharges within 180 seconds after administration ($p < 0.01$; Wilcoxon Rank-Sum test; N = 9 subjects treated), and cold saline irrigation decreased the frequency of general interictal discharges within 240 seconds after initiation ($p < 0.01$; Wilcoxon Rank-Sum test; N = 8 subjects treated; Fig. 2**D, 2E**). Surprisingly, these interventions did not significantly change local interictal discharges ($p > 0.01$; Wilcoxon Rank-Sum test).

The high-spatial-resolution PEDOT:PSS microelectrodes may allow us to decipher whether IIDs can "travel," particularly since multiple microelectrode contacts appeared to detect the same interictal discharge during a 2-second time window (Fig. 2**A, 2B**). To test whether we could observe distinct groups of traveling phenomena that create a "path," we temporally marked the interictal discharge's largest deflection points (e.g. the peak or valley) within a 2-second time window for each electrode and for each IID detection. To understand whether these "paths" could be grouped into specific patterns, we calculated the discrete Fréchet distance (Fig. 2**F**) and clustered values (Fig. 2**G**, **H**) to form groups with similar paths. This approach revealed that at least two paths, and often many more, could be clustered across IIDs for each subject when

Table 2
Detected general IIDs, local IIDs, IID paths, and HFOs in PEDOT:PSS recordings in each subject. Abbreviations: IIDs – interictal discharge; HFOs – high-frequency oscillations.

Subject #	Interictal Discharges				HFOs	
	General IIDs	Local IIDs	General IID Paths	Local IID Paths	Average HFOs Per Channel	Number of Clusters
1	32	0	3		117.2	12
2						
3						
4	2	2			58.6	5
5	118	2	8		360.5	31
6	50	0	5			
7	167	2	2		66.9	27
8	49	30	2	2	294.3	17
9	2	1			531.6	6
10						
11	48	0	7			
12	0	0			40.5	14
13	1	7			179.5	24
14	4	1				
15	2	0			65.8	5
16	9	0			70.4	2
17	1	5			340.3	16
18	108	35	4	2	26.1	2
19	7	22		2	147.6	8
20	13	2	4		31.1	1
21	136	6	28		162.7	1
22	193	47	30	9	114.1	15
	163	45	11	6	127.0	51
23	1	0			80.5	9
24	29	8	8		68.5	1
25	1	0			32.4	0
26	0	0			1.9	0
	3	0			3.5	0
27	4	0			5.3	0
28	11	0	5		9.3	2
29	1	0			0.8	0
	27	4	9		5.9	3
	9	3			1.0	0
30	69	13	13	3	0.5	0
	25	5	3		19.1	5

examining general IIDs; we found an average of 10.1 paths across subjects (Table 2, Fig. 2**C**, Fig. 2**I**). The overall average speed of these interictal discharges was 60 ± 3.5 mm/s (standard error of the mean, SEM).

3.3. High frequency oscillations (HFOs)

Fast ripple HFOs occurred in all included microelectrode recordings across patients (N = 24, Fig. 3**A**). There was no statistically significant difference in the number of HFOs detected in subjects who underwent general anesthesia versus monitored anesthesia care ($p > 0.05$, Wilcoxon Rank-Sum test). Overall, HFOs also responded to both cold saline and intravenous medication. Though medications known to promote interictal discharges (alfentanil or methohexital) raised HFOs' average frequency per channel over the baseline, this change was not statistically significant ($p > 0.05$, Wilcoxon Rank-Sum test, N = 9 subjects treated; Fig. 3**B**). On the other hand, HFOs became significantly less frequent 60 seconds after cold saline irrigation began ($p < 0.05$, Wilcoxon Rank-Sum test, N =8 subjects treated; Fig. 3**C**).

Because the PEDOT:PSS microelectrodes have high spatial resolution, they were able to reveal that HFOs may localize over specific microelectrode array sections in a single recording or subject (Fig. 3**D**). However, this analysis overlooked the temporal changes that may occur over the course of the recording. We found that specific portions of the underlying cortex tended to generate more HFOs during specific time windows. As a result, we used an approach, adapted from methodology used to study neuronal avalanches, that would show the spatiotemporal dynamics of these HFO detections (Fig. 3**E**). Examining HFO detection patterns in time windows across channels indicated that similar detection patterns in particular channels could be spatially clustered (Fig. 3**G**) into separate groups among channel subsets (Fig. 3**H-I**). With a threshold of $p \leq 0.001$, 88% of subjects demonstrated at least 1 unique HFO detection pattern that could not be explained by chance (as compared with a shuffled data set, Fig. 3**F**, Table 2). A family group involved a minimum of one electrode contact and a maximum of 96, with an average of 13.8, though the number of commonalities per electrode in each family group could differ (Fig. 3**H**). These results suggest that a generator's lowest spatial bound is < 50 μm (the intercontact distance) but also that, more often, HFO generation involves a larger, sometimes heterogenous, non-contiguous network of neuronal activity.

To determine if there was a temporal relationship between HFOs and IIDs, we performed cross-covariance calculations between the HFO times versus the IID peak times in the same recordings. For both general and local interictal discharges, HFO detections occurred significantly more often during the interictal discharge's rising phase, using a 0.2 s time window around the IID peak time across subjects ($p < 0.01$, Wilcoxon rank-sum, N = 24).

3.4. Periodic patterns and microseizures

Our analyses found rare examples of repeating interictal discharges, which are generally described as periodic discharges in a clinical setting. In two subjects, these localized patterns convincingly appeared in a few electrodes (Fig. 4**A, 4B**). Given their lack of significant evolution or spread, these patterns were ultimately considered to be periodic patterns rather than distinct seizure events, based on prior clinical definitions (Ebersole, 2014; Hirsch et al., 2021). Of the examples obtained in these two patients, the smallest distance involved on the electrode was 50 μm.

We also noted microseizure events in two participants. In one subject, who had history of seizures, two events were isolated primarily to one electrode with a surrounding field (Fig. 4**C-E**). These patterns' highest amplitude occurred in one electrode, and the frequency of their discharges clearly evolved, consistent with a seizure-type phenomenon. Though the microseizure event signal was highly localized, voltage fields were detected in neighboring electrodes up to 100 μm away. This event did not clinically manifest intraoperatively. The second patient exhibited a similar phenomenon, with localized epileptiform discharges primarily seen on one electrode with spread to the neighboring electrode contact, spanning a distance of 50 μm.

3.5. Multi-Unit activity (MUA)

We used the Kilosort software package (Pachitariu et al., 2016) to sort fast (>250 Hz) unitary events into separable clusters using a template matching approach that considers waveform shape and spatial spread across electrode sites (Fig. 5). In 16 out of 30 participants, we defined clusters of repeated unitary fast events that were consistent with multi-unit activity (MUA) and appeared similar to prior reports (Khodagholy et al., 2015). These fast events colocalized with both the general IIDs and HFOs in space (on the same electrode sites) and through time in single recordings (Fig. 5**A-C**).

To clarify whether there was a temporal relationship between this MUA and the IIDs and HFOs, we calculated the peri-stimulus time histogram (PSTH) of the MUA relative to the IIDs and HFOs, considered separately (Fig. 5**D**). We found PSTH value peaks around zero, indicating that some MUA occurred with the general IIDs and HFOs. To test this further, we evaluated the cross-covariance values between the general IID and MUA times (Fig. 5**E**) and the HFO and MUA times (Fig. 5**F**) across the data set. Next, to determine if there was a significant cross-covariance relationship, that was consistent across the data set, between IIDs or HFOs and MUA, we calculated whether the cross-covariance values differed significantly in pre-event time periods (Fig. 5**E-F**). Our results showed the peaks in the cross-covariance averages between the general IIDs and MUA were not significant relative to 5 seconds before the IIDs ($p > 0.05$; Wilcoxon Rank-sum test; N = 16; Fig. 5**E**). In contrast, the central peak in the cross-covariance averages between the HFOs and MUA was significant ($p < 0.05$, Wilcoxon Rank-sum test, false discovery rate controlled, N = 16; Fig. 5**E**). It is important to note, however, that this covariance was small; that is, many HFOs did not have corresponding MUA, and vice-versa, suggesting the algorithms were not detecting the same physiological event but rather two distinct events. In addition, this covariance relationship was not found between local IIDs and MUA in either the PSTH or the cross-covariance calculations (data not shown). This indicates that MUA co-varies with, and could occur at the same times as, HFOs in these high spatial and temporal resolution recordings, but we could not find a covarying or time-locked relationship between IIDs and MUA.

4. Discussion

We found that high-spatial-resolution recordings on the cortical surface can provide detailed information regarding microscale dynamics of epileptic electrophysiologic markers. Specifically, we found that IIDs can either involve both relatively large areas of cortex or be localized to regions as small as 50 μm. These events can also propagate through multiple, separable, identifiable paths over the cortical surface. Similarly, HFOs can be limited to microscale regions and repeat over time. The rare microseizure events we observed further illustrate the distinctly local nature of epileptic events. Overall, these findings indicate there may be irritative cortex microdomains, on the order of 50 μm, involved in the epileptic network. In addition, certain epileptiform events can only be cap-

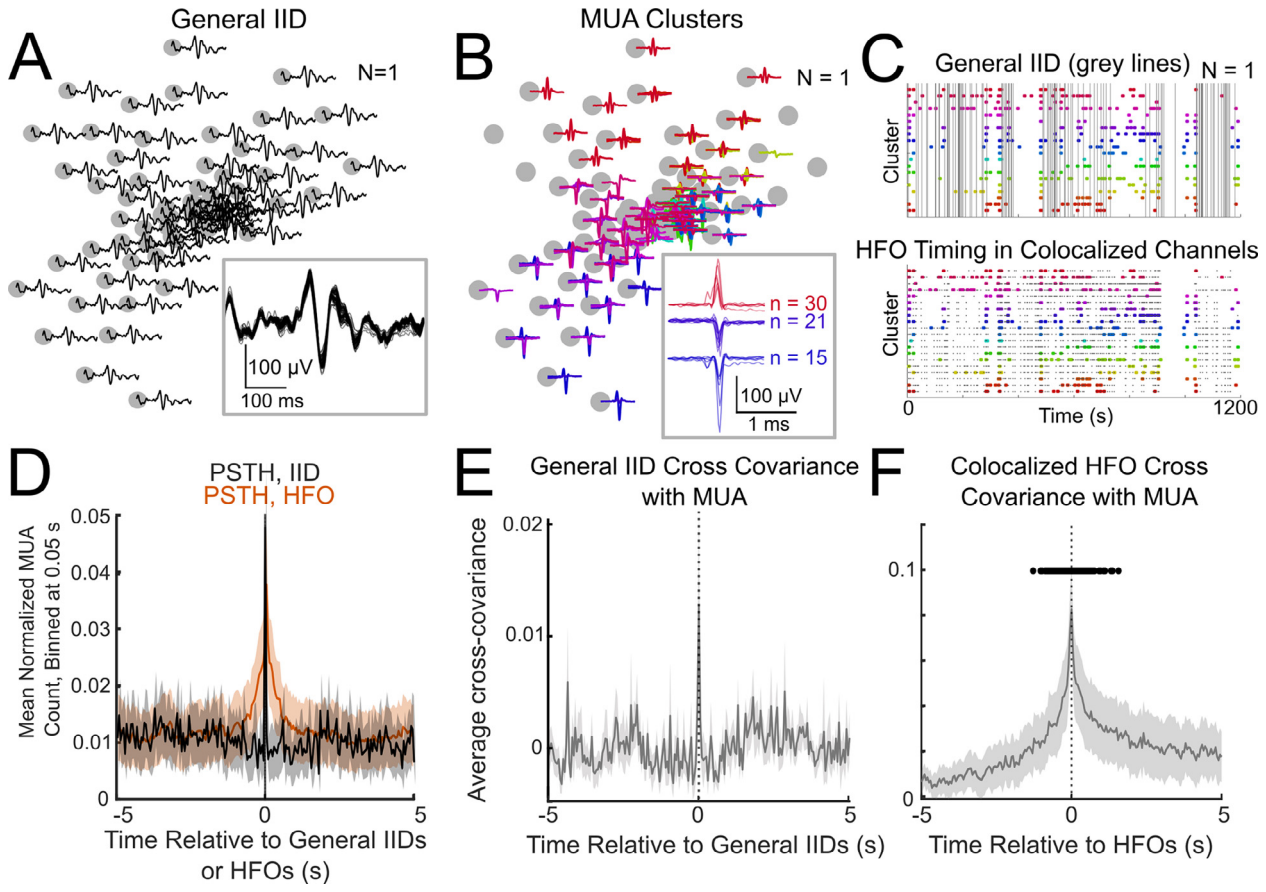

Fig. 5. Multi-Unit Activity (MUA). A) Sample spatial spread of a general interictal discharge (IID) across a circular grid (LFP filtered at < 1000 Hz). Inset: zoomed-in view of the IID with waveforms from across the array overlaid on one another. B) Sorted clusters of fast (>250 Hz) unitary waveforms, or multi-unity activity, as distributed across the same circular grid array as shown in A. Different color lines indicate different unitary event clusters. Inset: sample waveforms for a few clusters. C) Raster plot showing the same recording as in A and B, showing the timing of the MUA in B throughout the recording, alongside the simultaneous general IIDs (gray lines in the top plot) and detected high frequency oscillations (HFOs) (gray dots in the bottom plot) in the same recording. D) MUA were sorted using Kilosort (see 2.9 Evaluating Multi-Unit Activity (MUA)), pooled per recording similarly to MUA, and then compared to the timing of the general IIDs (black line) and HFOs (orange line) in peri-stimulus time histograms (PSTH). Lines are averages across recordings (after averaging PSTHs per recording). Shaded areas indicate standard error. E) The pooled MUA times were then covaried with the general IIDs per recording. The gray line is an average across recordings (after averaging cross-covariance curves per recording). Shaded areas indicate standard error. N = 16. F) The pooled MUA times were then covaried with detected HFOs per recording. Black dots indicate the cross-covariance values differ significantly from zero. (Wilcoxon Rank-sum test, $p < 0.05$, false discovery rate controlled). The gray line is an average across recordings (after averaging cross-covariance curves per recording). Shaded areas indicate standard error. N = 16. For (A) and (B), voltage tracings not shown represent electrodes that were removed due to exclusion criteria (see 2.5 Data Analysis and Data Exclusion Criteria) Abbreviations: IID – interictal discharge; HFO – high frequency oscillation; MUA – multi-unit activity; PSTH – peri-stimulus time histogram; n – number; N – number of subjects; V – volts; s – seconds.

tured with high-density electrode recordings, and our current typical recording approaches may be biased towards more widespread events. Because previously published works generally employed lower spatial resolution, these dimensions remain incompletely identified in human recordings.

Localized IIDs could correspond to previously reported microevents. In one group of studies, investigators observed these events using penetrating microelectrode semi-chronic recordings in an extraoperative environment (Schevon et al., 2010, 2008). With the NeuroPort array, which has 400 μm electrode spacing, Schevon and colleagues noted microdischarges, which were described as epileptiform discharges that could not be seen in adjacent clinical electrodes. This study documented events that occurred on only one microelectrode. Their results were bolstered by further review of the interictal data, which showed multiple populations of microdischarges (Schevon et al., 2010). Our study found similar evidence of these microdischarges, though in a different environment – the operating room – and using non-penetrative electrodes over eloquent regions. However, we did not see single-channel interictal discharges, reflecting the possibility that the PEDOT:PSS devices' tighter spatial pitch was actually below the smallest domain of epileptiform activity generation. The lower bound appears to be ~ 50 μm.

More importantly, by tracking these interictal discharges across the array, we found evidence that interictal discharges may take specific paths across the cortical surface, an observation which may suggest an underlying epileptic network that promotes interictal discharge progression across the cortex that is unique to each subject. Similar results have been previously noted at the macro scale (Sabolek et al., 2012) and in animal pharmacologic models (Vanleer et al., 2016). These IIDs were seen travelling at rates similar to those previously reported in animals (primarily in slice physiology), at 29 ± 18 mm/s (Trevelyan et al., 2007).

The particular paths taken by interictal discharges are thought to be secondary to specific neuronal responses along the path, coupled with the effects of intervening interneurons (Chizhov et al., 2019; Sabolek et al., 2012). In a clinical context, these propagation patterns have been used to identify pathologic regions from which IIDs emanate, though their ultimate impact on post-surgical outcome is not well defined (Alarcon et al., 1997; Tomlinson et al., 2016). Our method demonstrates that these discharges may in fact be further spatially resolved and highlights that how these dis-

charges travel over the cortical surface may be highly complex. Future work could involve mapping these paths, considering the locations of both the microelectrode array and nearby pathologic tissue, to determine whether predictable emanations from specific cortical areas match these IID clustered paths. In addition, further analyses should investigate how these paths interact with the spatiotemporal patterns of HFO detections. Ultimately, these advances may help characterize the underlying epileptic network, particularly on smaller scales, and support therapeutic efforts to modulate or interrupt it.

By using analyses typically employed to uncover repeating spatial and temporal patterns in neuronal avalanches, we demonstrate that fast-ripple HFOs can be detected over the cortical surface in unique, repeatable patterns. We investigated fast ripples because these phenomena are considered more indicative of pathologic activity (van Klink et al., 2014) although there remains some debate within the field (Bragin et al., 2002a; Chari et al., 2020; Weiss et al., 2016; Worrell et al., 2008; Zijlmans et al., 2012b). Multiple groups have reported that fast ripples can be extremely spatially localized, involving a single microelectrode (Schevon et al., 2009). While our data included similar examples of single-channel HFOs, we expand on these prior findings by showing that non-penetrative microelectrodes can detect HFOs and that specific non-contiguous areas of the cortical surface tend to fire in concert, perhaps indicating how particular regions of the cortical surface may be more epileptogenic or how different zones may be linked as part of an epileptic network. Similarly, our work also supports prior microelectrode-based HFO findings that proved focal HFOs can be identified in regions < 1 mm^3 (Worrell et al., 2008), but here we suggest the lower limit may be 50 μm. These results again highlight the complex underlying cortical architecture that can lead to epileptiform activity.

There are currently some limitations to how HFOs may be used to guide patient care. While some studies have shown that HFOs, particularly fast ripples, can inform the resection of epileptic regions that influence outcome (Hussain et al., 2017; Klink et al., 2014; Klooster et al., 2017), one prospective trial recently demonstrated that incorporating intraoperative HFO analysis can result in conflicting clinical data, which may indicate network phenomena linking HFOs (Jacobs et al., 2018). In addition, there has been concern that because fast ripples represent small areas of cortex, undersampling can occur with current clinical intraoperative macroelectrode recordings (Klooster et al., 2017). Furthermore, additional research in microelectrode recordings may be required to determine whether such relationships hold true under microelectrode, versus macroelectrode, recording conditions, though prior studies have suggested electrode contact size may not affect HFO detection ability (Châtillon et al., 2013).

Semi-chronic recordings have previously revealed the presence of microseizure events. Using a subdural electrode grid that included microelectrode contacts with 1 mm pitch, implanted in a semi-chronic setting, Stead and colleagues found examples of seizure-like events as well as interictal events that occurred on single microelectrodes (Stead et al., 2010). Further, Schevon and colleagues similarly found microseizures (Schevon et al., 2008). While our microelectrode data did show evidence of periodic patterns, these did not appear to organize or evolve sufficiently to be deemed seizure events, based on our described criteria. Nevertheless, we did identify microseizure events that were primarily localized to single contacts, with notable voltage spread to neighboring contacts. One benefit of our reduced spatial pitch is that it indicates these events occur over an approximately 100 μm spatial spread and appear to be more consistent with true events rather than artifacts.

The relative paucity of periodic discharges and microseizure events in our recordings may reflect the relatively short duration of our recordings and/or the fact that they were performed under either general anesthesia or sedation. Our recording times were limited due to the need to preserve high quality of patient care. By dampening overall cortical excitability, anesthesia may have reduced the possibility of capturing seizure events. Administering provoking medications, such as alfentanil and methohexital, was insufficient to definitively trigger microseizure events during our microelectrode recordings. Ultimately, because our study recordings were taken during surgery, there are limitations to how many events we could capture over time.

Of note, two subjects in our study did not have history of seizures, yet IIDs and HFOs (but not microseizures) were found in their microelectrode recordings. One of these subjects, number 19, was taking a prophylactic antiseizure medication, levetiracetam, due to clinical concern of lowered seizure threshold. This medication use could have prevented a clinical seizure, though underlying interictal activity could still be detected. The other subject, number 23, was not on antiseizure medication but had a history of astrocytoma. Multiple factors could have contributed to the presence of identifiable IIDs and HFOs in this subject, including use of anesthetic medications and changes in the tumor microenvironment. For instance, altering propofol dosing during a procedure can produce proconvulsive effects, clinical seizures, or seizure-like phenomena with epileptiform discharges (Koch et al., 2018; Sanjuan et al., 2010; Walder et al., 2002) or trigger changes in high frequency oscillations (Zijlmans et al., 2012a). Gliomas can be infiltrative and also change the host microenvironment in ways that can lead to epileptic discharges (Campbell et al., 2012; Pallud et al., 2014). Finally, IIDs (So, 2010) and HFOs (Blanco et al., 2011) are rarely found in healthy patients without seizure history.

Our work with multi-unit activity demonstrated a relationship with HFOs, but not with IIDs. Some reasons for this may include surface microelectrodes' inability to sample neural activity at depth, as well as the limited number of MUA clusters that were identified. With regard to single-unit activity and HFOs in humans, prior research has demonstrated that single units in the hippocampus exhibit firing changes during ripples (Quyen et al., 2008), a relationship that also extends to fast ripples (Jiruska et al., 2017; Köhling and Staley, 2011). Either synchronous or asynchronous action potential firing may represent cellular underpinnings for HFOs (Jiruska et al., 2017), and foundational work in HFOs has shown that fast ripples and unit activity are related in the mesial temporal lobe (Bragin et al., 2011, 2002b). This suggests detectable HFO activity may originate more locally than IID activity, which may require firing by a larger neural network. Heterogeneous, sparse populations could be involved in generating IIDs (Alvarado-Rojas et al., 2013), and given that a substantial fraction of neurons may not be involved in IIDs, the limited MUA clusters in our study may preclude our ability to find a definitive relationship. We recognize that our HFO detector cannot fully exclude possible high-frequency contamination caused by MUA activity, though how to interpret these findings remains an open question (Menendez de la Prida et al., 2015). Alternatively, our results may be explained by the microelectrode detecting both fast ripples and MUA activity at a local, superficial level. We recognize that, compared to prior foundational literature, we may be detecting neural activity from a different population of neurons, using a different recording methodology. Further analyses may additionally examine how stratifying HFOs into subgroups, such as those associated or not associated with IIDs, could lead to different covariances with MUA.

Exploring these phenomena further is limited by the electrode arrays' current spatial distribution; the circular grid covers approximately 4x4 mm and the bi-linear array spans about 3 mm. Thus, only small cortical surface areas could be sampled. This is a surmountable challenge as these electrodes can be scaled to cover

substantially larger areas (Chiang et al., 2020). An additional limitation is recording duration, as mentioned above, due to the intraoperative environment and need to ensure subject safety. We also understand that our clinical environment includes several additional variables that cannot be controlled as they relate directly to patient care, such as anesthesia type, medication usage, and recording location. While we did not see a statistically significant difference in IID or HFO detection when comparing conditions, for example in general anesthesia versus monitored anesthesia care, we recognize that there are likely several co-variables that could affect this finding and would require significantly larger numbers of subjects to allow for statistical power.

Nevertheless, even with these limitations, we were able to identify unique features of interictal discharges and high frequency oscillations using superficial microelectrode arrays that point to microscale anatomy of epileptiform activity. This has substantial implications for the basic physiology of epilepsy, how we detect, track and localize pathological activity and, ultimately, therapeutic options which focus on these microdomains of epileptiform neural action.

Declaration of Competing Interest

The authors declare that they have no known competing financial interests or personal relationships that could have appeared to influence the work reported in this paper.

Acknowledgement

We would like to thank Yangling Chou, Erica Johnson, and Gavin Belok for their assistance with data collection. We also thank Melissa Murphy, Aaron Tripp, and other intraoperative monitoring team members at BWH and MGH for their assistance with intraoperative clinical recordings. Finally, we would like to recognize the patients for their invaluable participation in the study.

This research was sponsored by the U.S. Army Research Office and Defense Advanced Research Projects Agency under Cooperative Agreement Number W911NF-14-2-0045. Additional support included ECOR and K24-NS088568 to SSC; NSF-CAREER award #1351980, NSF CMMI award #1728497, and NIH DP2-EB029757 to SAD. The views and conclusions contained in this document are those of the authors and do not represent the official policies, either expressed or implied, of the funding sources.

DPC has received consulting fees from Lilly and Boston Pharmaceuticals as well as honoraria and travel reimbursement from Merck for invited lectures and the NIH and DOD for reviewing clinical trials and grants.

Ethical Publication Statement

We confirm that we have read the Journal's position on issues involved in ethical publication and affirm that this report is consistent with those guidelines.

References

Alarcon G, Seoane JJG, Binnie CD, Miguel MCM, Juler J, Polkey CE, et al. Origin and propagation of interictal discharges in the acute electrocorticogram. Implications for pathophysiology and surgical treatment of temporal lobe epilepsy. Brain 1997;120:2259–82. https://doi.org/10.1093/brain/120.12.2259.

Alvarado-Rojas C, Lehongre K, Bagdasaryan J, Bragin A, Staba R, Engel J, Navarro V, Le Van Quyen M. Single-unit activities during epileptic discharges in the human hippocampal formation. Front Comput Neurosc 2013;7. https://doi.org/10.3389/fncom.2013.00140.

Beggs JM, Plenz D. Neuronal Avalanches Are Diverse and Precise Activity Patterns That Are Stable for Many Hours in Cortical Slice Cultures. J Neurosci 2004;24:5216–29. https://doi.org/10.1523/jneurosci.0540-04.2004.

Blanco JA, Stead M, Krieger A, Stacey W, Maus D, Marsh E, Viventi J, Lee KH, Marsh R, Litt B, Worrell GA. Data mining neocortical high-frequency oscillations in epilepsy and controls. Brain 2011;134(10):2948–59. https://doi.org/10.1093/brain/awr212.

Bragin A, Benassi SK, Kheiri F, Engel J. Further evidence that pathologic high-frequency oscillations are bursts of population spikes derived from recordings of identified cells in dentate gyrus. Epilepsia 2011;52:45–52. https://doi.org/10.1111/j.1528-1167.2010.02896.x.

Bragin A, Mody I, Wilson CL, Engel J. Local Generation of Fast Ripples in Epileptic Brain. J Neurosci 2002a;22(5):2012–21. https://doi.org/10.1523/JNEUROSCI.22-05-02012.2002.

Bragin A, Wilson CL, Staba RJ, Reddick M, Fried I, Engel J. Interictal high-frequency oscillations (80–500Hz) in the human epileptic brain: Entorhinal cortex. Ann Neurol 2002b;52(4):407–15. https://doi.org/10.1002/ana.v52:410.1002/ana.10291.

Burnos S, Frauscher B, Zelmann R, Haegelen C, Sarnthein J, Gotman J. The morphology of high frequency oscillations (HFO) does not improve delineating the epileptogenic zone. Clin Neurophysiol 2016;127(4):2140–8. https://doi.org/10.1016/j.clinph.2016.01.002.

Campbell SL, Buckingham SC, Sontheimer H. Human glioma cells induce hyperexcitability in cortical networks. Epilepsia 2012;53:1360–70. https://doi.org/10.1111/j.1528-1167.2012.03557.x.

Chari A, Thornton RC, Tisdall MM, Scott RC. Microelectrode recordings in human epilepsy: A case for clinical translation? Brain Commun 2020;2. https://doi.org/10.1093/braincomms/fcaa082. fcaa082-.

Châtillon CE, Zelmann R, Hall JA, Olivier A, Dubeau F, Gotman J. Influence of contact size on the detection of HFOs in human intracerebral EEG recordings. Clin Neurophysiol 2013;124:1541–6. https://doi.org/10.1016/j.clinph.2013.02.113.

Chiang C-H, Won SM, Orsborn AL, Yu KJ, Trumpis M, Bent B, Wang C, Xue Y, Min S, Woods V, Yu C, Kim BH, Kim SB, Huq R, Li J, Seo KJ, Vitale F, Richardson A, Fang H, Huang Y, Shepard K, Pesaran B, Rogers JA, Viventi J. Development of a neural interface for high-definition, long-term recording in rodents and nonhuman primates. Sci Transl Med 2020;12(538):eaay4682. https://doi.org/10.1126/scitranslmed.aay4682.

Chizhov AV, Amakhin DV, Zaitsev AV. Spatial propagation of interictal discharges along the cortex. Biochem Biophys Res Commun 2019;508(4):1245–51. https://doi.org/10.1016/j.bbrc.2018.12.070.

Cimbalnik J, Brinkmann B, Kremen V, Jurak P, Berry B, Gompel JV, Stead M, Worrell G. Physiological and pathological high frequency oscillations in focal epilepsy. Ann Clin Transl Neur 2018;5(9):1062–76. https://doi.org/10.1002/acn3.2018.5.issue-910.1002/acn3.618.

Dworetzky BA, Reinsberger C. The role of the interictal EEG in selecting candidates for resective epilepsy surgery. Epilepsy Behav 2011;20(2):167–71. https://doi.org/10.1016/j.yebeh.2010.08.025.

Ebersole JS, editor. Current Practice of Clinical Electroencephalography. Fourth Edition. Wolters Kluwer Health: Philadelphia, PA; 2014.

Eiter T, Mannila H. Computing Discrete Fréchet Distance. Tech. Rep. CD-TR 94/64, Christian Doppler Laboratory for Expert Systems. 1994.

Ganji M, Kaestner E, Hermiz J, Rogers N, Tanaka A, Cleary D, Lee SH, Snider J, Halgren M, Cosgrove GR, Carter BS, Barba D, Uguz I, Malliaras GG, Cash SS, Gilja V, Halgren E, Dayeh SA. Development and Translation of PEDOT:PSS Microelectrodes for Intraoperative Monitoring. Adv Funct Mater 2018;28(12):1700232. https://doi.org/10.1002/adfm.v28.1210.1002/adfm.201700232.

Gliske SV, Irwin ZT, Chestek C, Stacey WC. Effect of sampling rate and filter settings on High Frequency Oscillation detections. Clin Neurophysiol 2016;127(9):3042–50. https://doi.org/10.1016/j.clinph.2016.06.029.

Harrach MA, Mousavi H, Dieuset G, Ismailova E, Wendling F. Model-Guided Design of Microelectrodes for HFO Recording. Annu Int Conf IEEE Eng Med Biol Soc 2020;2020:3428–31. https://doi.org/10.1109/embc44109.2020.9176032.

Hermiz J, Rogers N, Kaestner E, Ganji M, Cleary D, Snider J, et al. A clinic compatible, open source electrophysiology system. Annu Int Conf IEEE Eng Med Biol Soc 2016;2016:4511–4. https://doi.org/10.1109/embc.2016.7591730.

Hirsch LJ, Fong MWK, Leitinger M, LaRoche SM, Beniczky S, Abend NS, et al. American Clinical Neurophysiology Society's Standardized Critical Care EEG Terminology: 2021 Version. J Clin Neurophysiol 2021;38:1–29. https://doi.org/10.1097/wnp.0000000000000806.

Hussain SA, Mathern GW, Hung P, Weng J, Sankar R, Wu JY. Intraoperative fast ripples independently predict postsurgical epilepsy outcome: Comparison with other electrocorticographic phenomena. Epilepsy Res 2017;135:79–86. https://doi.org/10.1016/j.eplepsyres.2017.06.010.

Jacobs J, Wu JY, Perucca P, Zelmann R, Mader M, Dubeau F, Mathern GW, Schulze-Bonhage A, Gotman J. Removing high-frequency oscillations. Neurology 2018;91(11):e1040–52. https://doi.org/10.1212/WNL.0000000000006158.

Janca R, Jezdik P, Cmejla R, Tomasek M, Worrell GA, Stead M, Wagenaar J, Jefferys JGR, Krsek P, Komarek V, Jiruska P, Marusic P. Detection of Interictal Epileptiform Discharges Using Signal Envelope Distribution Modelling: Application to Epileptic and Non-Epileptic Intracranial Recordings. Brain Topogr 2015;28(1):172–83. https://doi.org/10.1007/s10548-014-0379-1.

Jefferys JGR, Menendez de la Prida L, Wendling F, Bragin A, Avoli M, Timofeev I, Lopes da Silva FH. Mechanisms of physiological and epileptic HFO generation. Prog Neurobiol 2012;98(3):250–64. https://doi.org/10.1016/j.pneurobio.2012.02.005.

Jiruska P, Alvarado-Rojas C, Schevon CA, Staba R, Stacey W, Wendling F, Avoli M. Update on the mechanisms and roles of high-frequency oscillations in seizures and epileptic disorders. Epilepsia 2017;58(8):1330–9. https://doi.org/10.1111/epi.2017.58.issue-810.1111/epi.13830.

Keller CJ, Truccolo W, Gale JT, Eskandar E, Thesen T, Carlson C, et al. Heterogeneous neuronal firing patterns during interictal epileptiform discharges in the human cortex. Brain 2010;133:1668–81. https://doi.org/10.1093/brain/awq112.

Khodagholy D, Gelinas JN, Thesen T, Doyle W, Devinsky O, Malliaras GG, Buzsáki G. NeuroGrid: recording action potentials from the surface of the brain. Nat Neurosci 2015;18(2):310–5. https://doi.org/10.1038/nn.3905.

Khodagholy D, Gelinas JN, Zhao Z, Yeh M, Long M, Greenlee JD, Doyle W, Devinsky O, Buzsáki G. Organic electronics for high-resolution electrocorticography of the human brain. Sci Adv 2016;2(11):e1601027. https://doi.org/10.1126/sciadv.1601027.

van Klink N, Frauscher B, Zijlmans M, Gotman J. Relationships between interictal epileptic spikes and ripples in surface EEG. Clin Neurophysiol 2016;127(1):143–9. https://doi.org/10.1016/j.clinph.2015.04.059.

van Klink NEC, van't Klooster MA, Zelmann R, Leijten FSS, Ferrier CH, Braun KPJ, van Rijen PC, van Putten MJAM, Huiskamp GJM, Zijlmans M. High frequency oscillations in intra-operative electrocorticography before and after epilepsy surgery. Clin Neurophysiol 2014;125(11):2212–9. https://doi.org/10.1016/j.clinph.2014.03.004.

van 't Klooster MA, van Klink NEC, Zweiphenning WJEM, Leijten FSS, Zelmann R, Ferrier CH, van Rijen PC, Otte WM, Braun KPJ, Huiskamp GJM, Zijlmans M. Tailoring epilepsy surgery with fast ripples in the intraoperative electrocorticogram. Ann Neurol 2017;81(5):664–76. https://doi.org/10.1002/ana.v81.510.1002/ana.24928.

Koch S, Rupp L, Prager C, Mörgeli R, Kramer S, Wernecke KD, Fahlenkamp A, Spies C. Incidence of epileptiform discharges in children during induction of anaesthesia using Propofol versus Sevoflurane. Clin Neurophysiol 2018;129(8):1642–8. https://doi.org/10.1016/j.clinph.2018.05.013.

Köhling R, Staley K. Network mechanisms for fast ripple activity in epileptic tissue. Epilepsy Res 2011;97(3):318–23. https://doi.org/10.1016/j.eplepsyres.2011.03.006.

Pachitariu M, Steinmetz N, Kadir S, Carandini M, Harris K. Fast and accurate spike sorting of high-channel count probes with KiloSort. Adv Neural Inf Process Syst 2016:1–9.

Pallud J, Quyen MLV, Bielle F, Pellegrino C, Varlet P, Labussiere M, et al. Cortical GABAergic excitation contributes to epileptic activities around human glioma. Sci Transl Med 2014;6:244ra89. https://doi.org/10.1126/scitranslmed.3008065.

Paulk AC, Yang JC, Cleary DR, Soper DJ, Halgren M, O'Donnell AR, et al. Microscale Physiological Events on the Human Cortical Surface. Cereb Cortex 2021. https://doi.org/10.1093/cercor/bhab040.

Lévesque M, Salami P, Gotman J, Avoli M. Two Seizure-Onset Types Reveal Specific Patterns of High-Frequency Oscillations in a Model of Temporal Lobe Epilepsy. J Neurosci 2012;32(38):13264–72. https://doi.org/10.1523/JNEUROSCI.5086-11.2012.

Menendez de la Prida L, Staba RJ, Dian JA. Conundrums of High-Frequency Oscillations (80–800 Hz) in the Epileptic Brain. J Clin Neurophysiol 2015;32(3):207–19. https://doi.org/10.1097/WNP.0000000000000150.

Le Van Quyen M, Bragin A, Staba R, Crepon B, Wilson CL, Engel J. Cell Type-Specific Firing during Ripple Oscillations in the Hippocampal Formation of Humans. J Neurosci 2008;28(24):6104–10. https://doi.org/10.1523/JNEUROSCI.0437-08.2008.

Ribeiro TL, Ribeiro S, Copelli M. Repertoires of Spike Avalanches Are Modulated by Behavior and Novelty. Front Neural Circuit 2016;10:16. https://doi.org/10.3389/fncir.2016.00016.

Sabolek HR, Swiercz WB, Lillis KP, Cash SS, Huberfeld G, Zhao G, Ste. Marie L, Clemenceau S, Barsh G, Miles R, Staley KJ. A Candidate Mechanism Underlying the Variance of Interictal Spike Propagation. J Neurosci 2012;32(9):3009–21. https://doi.org/10.1523/JNEUROSCI.5853-11.2012.

Salami P, Lévesque M, Gotman J, Avoli M. A comparison between automated detection methods of high-frequency oscillations (80–500Hz) during seizures. J Neurosci Meth 2012;211(2):265–71. https://doi.org/10.1016/j.jneumeth.2012.09.003.

San-juan D, Chiappa KH, Cole AJ. Propofol and the electroencephalogram. Clin Neurophysiol 2010;121(7):998–1006. https://doi.org/10.1016/j.clinph.2009.12.016.

Schevon CA, Goodman RR, McKhann G, Emerson RG. Propagation of Epileptiform Activity on a Submillimeter Scale. J Clin Neurophysiol 2010;27:406–11. https://doi.org/10.1097/wnp.0b013e3181fdf8a1.

Schevon CA, Ng SK, Cappell J, Goodman RR, McKhann G, Waziri A, et al. Microphysiology of Epileptiform Activity in Human Neocortex. J Clin Neurophysiol 2008;25:321–30. https://doi.org/10.1097/wnp.0b013e31818e8010.

Schevon CA, Trevelyan AJ, Schroeder CE, Goodman RR, McKhann G, Emerson RG. Spatial characterization of interictal high frequency oscillations in epileptic neocortex. Brain 2009;132:3047–59. https://doi.org/10.1093/brain/awp222.

Sessolo M, Khodagholy D, Rivnay J, Maddalena F, Gleyzes M, Steidl E, Buisson B, Malliaras GG. Easy-to-Fabricate Conducting Polymer Microelectrode Arrays. Adv Mater 2013;25(15):2135–9. https://doi.org/10.1002/adma.201204322.

Siegle JH, López AarónC, Patel YA, Abramov K, Ohayon S, Voigts J. Open Ephys: an open-source, plugin-based platform for multichannel electrophysiology. J Neural Eng 2017;14(4):045003. https://doi.org/10.1088/1741-2552/aa5eea.

So EL. Interictal Epileptiform Discharges in Persons Without A History of Seizures: What Do They Mean? J Clin Neurophysiol 2010;27:229–38. https://doi.org/10.1097/wnp.0b013e3181ea42a4.

Stead M, Bower M, Brinkmann BH, Lee K, Marsh WR, Meyer FB, et al. Microseizures and the spatiotemporal scales of human partial epilepsy. Brain 2010;133:2789–97. https://doi.org/10.1093/brain/awq190.

Tomlinson SB, Bermudez C, Conley C, Brown MW, Porter BE, Marsh ED. Spatiotemporal Mapping of Interictal Spike Propagation: A Novel Methodology Applied to Pediatric Intracranial EEG Recordings. Front Neurol 2016;7:229. https://doi.org/10.3389/fneur.2016.00229.

Trevelyan AJ, Baldeweg T, van Drongelen W, Yuste R, Whittington M. The Source of Afterdischarge Activity in Neocortical Tonic-Clonic Epilepsy. J Neurosci 2007;27(49):13513–9. https://doi.org/10.1523/JNEUROSCI.3005-07.2007.

Vanleer AC, Blanco JA, Wagenaar JB, Viventi J, Contreras D, Litt B. Millimeter-scale epileptiform spike propagation patterns and their relationship to seizures. J Neural Eng 2016;13(2):026015. https://doi.org/10.1088/1741-2560/13/2/026015.

Walder B, Tramèr MR, Seeck M. Seizure-like phenomena and propofol. Neurology 2002;58:1327–32. https://doi.org/10.1212/wnl.58.9.1327.

Wang S, So NK, Jin B, Wang IZ, Bulacio JC, Enatsu R, et al. Interictal ripples nested in epileptiform discharge help to identify the epileptogenic zone in neocortical epilepsy. Clin Neurophysiol 2017;128:945–51. https://doi.org/10.1016/j.clinph.2017.03.033.

Wang S, Wang IZ, Bulacio JC, Mosher JC, Gonzalez-Martinez J, Alexopoulos AV, et al. Ripple classification helps to localize the seizure-onset zone in neocortical epilepsy. Epilepsia 2013;54:370–6. https://doi.org/10.1111/j.1528-1167.2012.03721.x.

Weiss SA, Alvarado-Rojas C, Bragin A, Behnke E, Fields T, Fried I, et al. Ictal onset patterns of local field potentials, high frequency oscillations, and unit activity in human mesial temporal lobe epilepsy. Epilepsia 2016;57:111–21. https://doi.org/10.1111/epi.13251.

Wellman SM, Eles JR, Ludwig KA, Seymour JP, Michelson NJ, McFadden WE, et al. A Materials Roadmap to Functional Neural Interface Design. Adv Funct Mater 2018:28. https://doi.org/10.1002/adfm.201701269.

Wilke C, Drongelen Wvan, Kohrman M, He B. Identification of epileptogenic foci from causal analysis of ECoG interictal spike activity. Clin Neurophysiol 2009;120(8):1449–56. https://doi.org/10.1016/j.clinph.2009.04.024.

Worrell G, Gotman J. High-frequency oscillations and other electrophysiological biomarkers of epilepsy: clinical studies. Biomark Med 2011;5(5):557–66. https://doi.org/10.2217/bmm.11.74.

Worrell GA, Gardner AB, Stead SM, Hu S, Goerss S, Cascino GJ, et al. High-frequency oscillations in human temporal lobe: simultaneous microwire and clinical macroelectrode recordings. Brain 2008;131:928–37. https://doi.org/10.1093/brain/awn006.

Zijlmans M, Huiskamp GM, Cremer OL, Ferrier CH, van Huffelen AC, Leijten FSS. Epileptic high-frequency oscillations in intraoperative electrocorticography: The effect of propofol. Epilepsia 2012a;53:1799–809. https://doi.org/10.1111/j.1528-1167.2012.03650.x.

Zijlmans M, Jiruska P, Zelmann R, Leijten FSS, Jefferys JGR, Gotman J. High-frequency oscillations as a new biomarker in epilepsy. Ann Neurol 2012b;71(2):169–78. https://doi.org/10.1002/ana.v71.210.1002/ana.22548.